A Traction Substation State Estimator for Integrating Smart Loads in Transportation Grids Without the Need for Additional Sensors

Diab, I.; Chandra Mouli, G.R.; Bauer, P.

DOI
10.1109/TITS.2023.3317375

Publication date
2023

Document Version
Final published version

Published in
IEEE Transactions on Intelligent Transportation Systems

A Traction Substation State Estimator for Integrating Smart Loads in Transportation Grids Without the Need for Additional Sensors

Ibrahim Diab, *Member, IEEE*, Gautham Ram Chandra Mouli, *Member, IEEE*, and Pavol Bauer, *Senior Member, IEEE*

***Abstract*— Public electric transport grids tend to be oversized and underutilized. Therefore, they can become sustainable and multi-functional backbones to the city AC grid by integrating smart grid elements into their infrastructures. However, integrating smart grid loads and renewables requires a large array of wirelessly communicating sensors across the traction substations, the smart grid components, and each vehicle of the transport fleet. This can be both costly and technically complex. This paper proposes an analytical state estimator that can predict vehicle traffic count and spare power capacity under a traction substation without the use of any additional sensors. The estimator uses existing, locally available measurements at any power node on the traction section to inform the decision-making of the power management scheme at that node. Validating the results with up to 100000 stochastic test simulations of a verified traction grid model, up to 76% of the monitored conditions were detected, with no false positives, and without the need for additional sensors and wireless communication.**

***Index Terms*— Modeling, power management, smart grids, state estimators, transportation.**

NOMENCLATURE

$\alpha_n, \beta_n, \gamma_n$	Terms of the general solution for the node voltage.
ΔV_{real}	Real voltage drop without simplifications (impedance calculation).
ΔV_n	Change in voltage of node n.
$\epsilon_{\text{R}}, \epsilon_{\text{p}}$	Simple and propagated errors from the line impedance simplification.
Γ	Product of node power and line impedance.
$\hat{I}$	Peak current expected from a node.
λ, l_1, L	Length fragments use for impedance calculation.
$\mathscr{R}_\sigma$	Real impedance value between the substation and the node (no simplification).
ϕ	Normalized position with a paralleled section (impedance calculation).
ρ	Line impedance in Ω/m.
A	Area of zones used in the cone calculation.
C	Count of desired cases used in the cone calculation.
N	Number of nodes present on a section.
p	Number of parallel lines (impedance calculation).
P^*	Desired spare capacity
P_{r}	Rated substation capacity
$P_{\text{spare}}\Big\vert_{n=1}$	Spare capacity when the node of interest is the first node (closest to the substation).
R_σ, P_σ	Node states when the node is single (alone).
$R_{\text{M}}, I_{\text{M}}$, $V_{\text{M}}, P_{\text{M}}$	Measured node states.
t	Time.
V_σ, I_σ	Expected node states when the node is single (alone).
V_{N2F}	N2front voltage threshold signaling *at least* three nodes on the section.
$V_{\text{P*}}$	Node voltage threshold for spare capacity P^*.
$V_{\text{s}}, I_{\text{s}}$	Substation nominal voltage and substation supplied current.
$V_{\text{U}}, V_{\text{L}}$	Upper and lower voltage thresholds (cone).
V_{ZP}	Voltage at the zero spare capacity line.
$v_k, \hat{v}$	Node velocity and maximum velocity.
$V_{k,0}, V_{n,0}$	Initial voltage value for nodes k (all nodes but the node of interest n) and for node n, respectively.
$X_{k,0}$	Initial voltage value for nodes k (all nodes but the node of interest n).

Manuscript received 18 April 2023; revised 4 July 2023 and 23 August 2023; accepted 15 September 2023. Date of publication 5 October 2023; date of current version 18 April 2024. This work was supported by the Trolley 2.0 Project from Electric Mobility Europe. The Associate Editor for this article was Y. Kim. *(Corresponding author: Ibrahim Diab.)*

The authors are with the Electrical Sustainable Energy Department, TU Delft, 2628 CD Delft, The Netherlands (e-mail: i.diab@tudelft.nl).

Digital Object Identifier 10.1109/TITS.2023.3317375

I. INTRODUCTION

A. The Integration of Smart Loads in Transportation Networks

URBAN electric public transport networks have tremendous potential for providing more smart loads by integrating these into their infrastructures [1], [2], [3], [4], [5], [6], [7], [8]. This is because these grids are historically sized for the worst-case power demand scenarios and can be better utilized by smart loads and proper power management [9]. The infrastructure of these grids is made up of sections typically 1-2 km in length, fed by rectifier traction substations. Since

the accelerating vehicles (tram, trolleybus, etc.) can consume up to 3-5 times the load of a driving vehicle [1], [6], [7], [10], [11], [12], [13], the rectifier traction substations are oversized to cater to the rare possibility of a few unscheduled vehicles accelerating together under the supply zone of one substation. On the other hand, vehicle timetabling creates infrequent vehicle traffic under each traction substation, leaving large amounts of unused reserved grid capacity.

Many works are already rethinking these transport networks as multi-functional, active grids by integrating into them renewable energy sources (RES), storage systems, EV chargers, more sophisticated vehicle fleets (like In-Motion-Charging trolleybuses), and other smart loads [2], [3], [4], [5], [11], [13], [14], [15], [16], [17], [18], [19], [20], [21], [22], [23], [24], [25], [26], [27]

B. The Need for a Traction-Grid State Estimator

Despite having an underutilized spare energy capacity, traction grids can frequently have short periods of power congestion problems. These moments should be considered when integrating smart loads such as EV chargers so as not to violate the traction substation power rating, maximum line current, or minimum line voltage limitations.

Consequently, tapping into the unused capacity of these grids requires intelligent power management schemes and ample information on the traction grid state. These systems are even more complex because the loads constantly vary not only in power demand but also in location, which can affect the line voltage, transmission power losses, and line currents. Therefore, gathering the necessary grid state information requires a large array of wireless communication sensors communicating between themselves, with the traction substation, and with a local data processor for each grid supply zone.

Prediction models are, of course, not a new topic. The most common of these methods is the Kalman Filtering [28], which is a set of mathematical equations for estimating the state of a discrete-data controlled process from measurements that are typically noisy via a recursive computational methodology. Given its recursive nature, Kalman Filtering is not suited for estimating the traffic and spare power conditions of a galvanically isolated transport grid section as each instant of the system is not dependent (read: predictable) on its previous iteration. For example, a vehicle can suddenly brake at a traffic light or exit the substation supply zone, creating a traffic and power demand situation that is not necessarily predictable from its previous states. In more mathematical terms, there is no information to be confidently inferred from a state derivative. Moreover, Kalman Filters assume linearity and Gaussian distributions for both the system dynamics and measurement noise, which is not an assumption that can be afforded in stochastic traction networks that run with urban traffic. Finally, the models are typically linear and require large memory space for storing the covariance matrix.

Other methods, such as Artificial Neural Networks [29], are inspired by the structure and function of the human brain, designed to recognize patterns and relationships in data. However, these methods are computationally and resource (data) intensive. They also need a comprehensive and well-distributed set of data for the training, and the overfitting that can come from this is a consequence of their black-box approach.

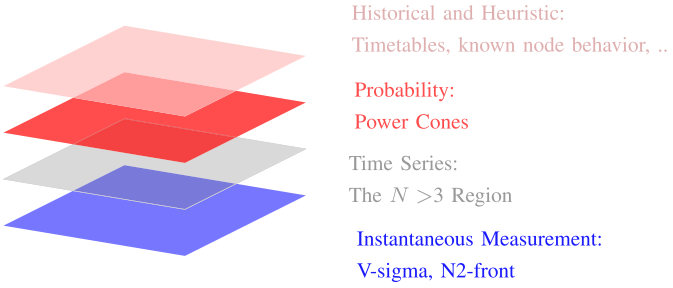

Fig. 1. The (possible) layers of the grid state estimator presented in this paper. Both the computational complexity and yet also the grid state information increase as the user decides to include more layers from bottom to top.

While other methods can be more analytical, such as in [30], [31], [32], they again are not suited for traction grids in particular as they struggle with changes to the system (for example, adding an EV charger or change in bus scheduling), scalability, and overfitting. There is then a need for a grid state estimator for traction grids that does not adopt a black-box approach and is both computationally simple and scalable.

C. The Proposed Grid State Estimator

Conveniently, some information is already available at each node (vehicle or smart load) because of the smart protection systems (e.g., measurements of overhead connection point voltage, current, and node power) and of vehicle live position sensing (GPS tracking for user apps, for example).

This paper aims to use only the already-available local data at a power node to estimate the traction substation's state and the number of other nodes present on the same traction grid section. This state estimation can be then used to better manage and integrate smart loads and renewables into traction networks and render them more sustainable, better utilized, and multi-functional.

Figure 1 explains the layers of the grid state estimator presented in this paper. Both the computational complexity and yet also the grid state information increase as the user decides to include more layers from bottom to top.

D. Paper Contributions

The paper offers the following contributions:

1) A traction grid state estimator able to estimate the number of nodes (traffic) present on a traction grid supply zone without the need for additional sensors or wireless communication among them
2) A traction grid state estimator to estimate the instantaneous power load demand on a traction substation to find the spare grid capacity for the power management of smart grid components in transport grids, without the need for additional sensors and wireless communication among them
3) A proposed methodology for estimating the node order on a traction grid supply zone to detect the presence of a node between the node of interest and the substation

without the need for additional sensors and wireless communication among them

4) A list of proposed applications of the proposed traction grid state estimator for the power management of smart loads in traction grids

E. Paper Structure

This paper started by motivating the need for the proposed traction grid state estimator. Section II explains the methodology used for testing the sets of equations and conditions that make up this estimator.

The first of these sets is presented in section III with the V-sigma condition that allows the detection of the presence of more than one power-consuming node on the studied supply zone (for example, more than one vehicle).

Section IV presents the N2-front used to detect the presence of more than two power-consuming nodes (for example, two vehicles or a vehicle and an EV charger in operation).

Section V presents the N3-region, which can be used to detect the presence of more than three nodes and to reason the node order (which node is closer to the substation).

The node order has an application in Section VI that more generally details the method for estimating the traction grid spare capacity.

Then, section VII offers a set of stochastic simulations to validate the proposed methods in this paper.

Beyond the theoretical investigations in this paper, Sections VIII and IX propose a number of extensions and power management applications of this estimator for smart load integration in traction grids, and finally, section X closes with conclusions and future works.

II. Methodology

A. Designed Test Conditions for the Stochastic Simulations in This Paper: DTC

While the estimator offered in this paper can be extended to any traction network, the examples and validations given to the developed theory here will study trolleygrid scenarios for the sake of an example.

Unless otherwise stated, the examples and validation cases in this paper use the here-defined Designed Test Conditions (DTC) based on the trolleygrid of Arnhem, the Netherlands (explained in [1]). These conditions are:

- A constant traction substation of 700V nominal voltage, V_s with a rated power capacity, P_r, of 800kW and a negligible length of the substation feeder cable, connected at the start of the section
- A standard overhead line of 0.172Ω/km, paralleled (also known as *equipotential lines*) in sets of 2 [1], [10], [11]
- A section of 1200m with nodes (bus, storage, etc.) always in load mode, between 0 and 300kW
- The maximum operating conditions are defined as a node drawing 500A and moving at a speed of 15m/s [1], [2], [10]

Furthermore, the scenarios studied in this paper are presented with line diagrams, of which the legend is in Figure 2:

- A (green) substation node of known nominal voltage and position at the start of a traction section

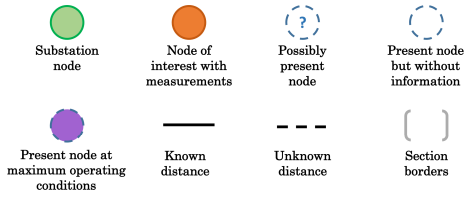

Fig. 2. Legend for the diagrams of the designed scenarios.

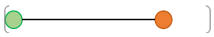

Fig. 3. The case of a single node at a known distance from the substation.

- A node of interest (orange) at a known distance and operating conditions. This is the node that is assumed to be using the estimator and has measurements of voltage, power, current, and position
- Other possibly present nodes (dashed circles with a question mark) at an unknown distance(s). These nodes can either be at unknown operating conditions (white) or assumed to be operating at maximum operating conditions (purple). If a node is already known to be present on the section, regardless of the information on its operational condition, it does not have a question mark in its representation

B. Traction Grid Calculation Model

The numerical simulations used in the examples and validations of this paper use a peer-reviewed and verified trolleygrid model detailed in [1], validated with data from the trolleygrid of Arnhem, the Netherlands. The model is based on the forward/backward sweep numerical method.

III. The $N>1$ Condition

A. Case of a Single Node on the Section (N=1)

Assume a node of interest alone on the section, at a known distance from the substation, that can be expressed by an overhead impedance of R_σ (Figure 3). The substation voltage is V_s. Since the work in [1] has already verified that the line impedance can be assumed as purely resistive in steady-state calculations, it can be said that:

$$V_\sigma = V_s - R_\sigma I_\sigma = V_s - R_\sigma \frac{P_\sigma}{V_\sigma} \tag{1}$$

where V_σ, I_σ, and P_σ are the voltage, current, and power of the single node, respectively. Which, when multiplied by V_σ, produces a quadratic equation, the solution of which is

$$V_\sigma = \frac{V_s + \sqrt{V_s^2 - 4R_\sigma P_\sigma}}{2} \tag{2}$$

This equation serves as a general definition of V_σ as the voltage at a node of interest when it is -or would have been- alone on a section. This definition can also be written as

$$V_\sigma \triangleq \frac{V_s + \sqrt{V_s^2 - 4\Gamma_\sigma}}{2} \tag{3}$$

where Γ_σ is defined as

$$\Gamma_\sigma \triangleq R_\sigma P_\sigma \tag{4}$$

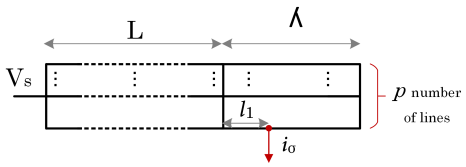

Fig. 4. Nomenclature of the variables used in the analysis of the error caused in the voltage calculation by the equivalent parallel impedance assumption.

This alternative form is useful for later derivations in this paper when re-arranging Eq.3 so that Γ_σ can be written in terms of the grid parameters as:

$$\Gamma_\sigma = V_\sigma (V_\mathrm{s} - V_\sigma) \tag{5}$$

B. The Nodal Voltage Estimation Error Caused by the Equivalent Impedance Approach to Parallel Lines

It is important at this stage to re-visit an implicit assumption made at the beginning in calculating the equivalent overhead line impedance, R_σ, by using a lumped impedance of the overhead feed and return line and the parallel overhead lines. The parallel lines (also called equipotential lines) are the paralleling of the sets of overhead feed and return cables to reduce the overall impedance by creating more paths for the current. The work in [1] flags the potential error from the lumped calculation approach and invites further investigation of it here.

Assume a trolleygrid section with p parallel lines, connected every λ meter (see Figure 4). The line resistance per unit length is ρ in Ω/m. A power-consuming node is alone on the section and at a position l_1 between two consecutive parallel lines after a distance L of an integer multiple of paralleled portions. In simpler words, the node is at $L + l_1$ meters from the substation. The substation is at voltage V_s, and the node is drawing a current I_σ.

For better readability in the following derivations, define the normalized bus position within a paralleled section, ϕ, as:

$$\phi \triangleq \frac{l_1}{\lambda} \tag{6}$$

Without the lumped equivalent-impedance assumption, the real voltage drop, ΔV_real, between the substation and the node is

$$\Delta V_\mathrm{real} = 2\rho \left[\phi\lambda \left(\frac{p - \phi(p-1)}{p} \right) + \frac{L}{p} \right] \cdot I_\sigma \tag{7}$$

And the actual equivalent resistance between the node and the station, defined here as $\mathcal{R}_\sigma$, is given accurately by the term:

$$\mathcal{R}_\sigma = 2\rho \left[\phi\lambda \left(\frac{p - \phi(p-1)}{p} \right) + \frac{L}{p} \right] \tag{8}$$

Meanwhile, the simplified equivalent resistance between the station and the node, R_σ, is given by:

$$R_\sigma \approx 2\rho \left(\frac{L + l_1}{p} \right) = 2\rho \left(\frac{L + \phi\lambda}{p} \right) \tag{9}$$

The error in the resistance value, ϵ_R, caused by the simplification in the resistance can be therefore quantified as:

$$\epsilon_\mathrm{R} \triangleq \mathcal{R}_\sigma - R_\sigma = 2\rho \left(\frac{p-1}{p} \right) \phi(1-\phi)\lambda \tag{10}$$

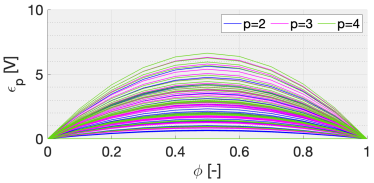

Fig. 5. The voltage computation error, ϵ_p, as a function of the normalized bus position within a paralleled section, ϕ, for a different number of paralleled lines, p. Each curve looks at a different scenario with L going from 0 to 1200m, λ from 100 to 300m, and the remaining variables at DTC.

Moreover, the sensitivity of the nodal voltage to the node impedance value is given by the partial derivative

$$\frac{\partial V_\sigma}{\partial R} = \frac{-P_\sigma}{\sqrt{V_\mathrm{s}^2 - 4\mathcal{R}_\sigma P_\sigma}} \tag{11}$$

Thereby, the error, ϵ_p, inflicted on V_σ by an error in the line resistance calculation can be quantified by the Propagation of Errors method [33] as:

$$\epsilon_\mathrm{p} = \left| \frac{\partial V_\sigma}{\partial R} \right| \cdot \epsilon_\mathrm{R} = 2 \left(\frac{p-1}{p} \right) \frac{\rho\lambda\phi(1-\phi)P_\sigma}{\sqrt{V_\mathrm{s}^2 - 4\mathcal{R}_\sigma P_\sigma}} \tag{12}$$

The above Eq.12 provides an estimate of the calculated voltage error expected as a function of P_σ as most of the terms in the equation are constant and known for a grid. Of course, the built infrastructure can sporadically differ from the design parameters because of constraints such as intersections and power pole positioning. Consequently, the precise value of λ - and thereby of ϕ and L- cannot always be guaranteed and would be an estimation. Luckily, considering the array of possible combinations of all the Eq.12 parameters (Figure 5), the error is predominately contained and under 6V. This allows the proposition of the "V-sigma condition" presented in the coming subsection.

C. Application of the Results: The V-Sigma Condition

A key grid state can be derived from the calculation of V_σ. Per definition, the V-sigma voltage is the voltage expected when a node is *alone* on a section. This value can be calculated, as shown previously, to an accuracy of ϵ_p. It follows logically then that if a measured nodal voltage, V_M, were to be outside of this range, the studied node is not alone on the section, and there is *at least* one other node.

However, because of the welcomed sharing of braking energy between nodes, it is advised to shy away from assuming that a measured nodal voltage, V_M, that is (almost) equal to V_σ implies that the node is alone on the section. This mathematical coincidence can arise from the fact that some nodes are supplying power, and thereby masking some of the expected voltage drop effects of other nodes. Also, a vehicle/node could be momentarily not drawing power or close enough to the section feed-in point that it is not causing an observable voltage drop. This is again a motivation to not interpret $V_\mathrm{M} \approx V_\sigma$ as a sign that a node is indeed alone on the section -that is to say:

$$\begin{cases} N > 1, & \text{if } V_\mathrm{M} \notin [V_\sigma - \epsilon_\mathrm{p}, V_\sigma[\\ \text{No information}, & \text{if otherwise} \end{cases} \tag{13}$$

Fig. 6. The case of a node of interest as the first node and at a known position with only one other node, which is at an unknown position, but at the maximum operating conditions.

IV. The $N > 2$ Front

A. Study of Two Nodes on a Section (N=2)

Consider a node of interest at an impedance R_M from the substation and drawing a power P_M (or, say, current I_M), such as in Figure 6. Notice that the subscript σ is not used as this no longer concerns the case of a single node and is replaced by M as an abbreviation for Measurement Node. Additionally, one node at an impedance R is drawing the maximum allowed node current of $\hat{I}$. For example, for a trolleybus, $\hat{I} = 500$A, and for a metro, the value is about 3900A. This is the limit imposed by the overhead current collector [1], [2].

It follows then from Kirchhoff's voltage law that:

$$V_M = \begin{cases} V_s - R\hat{I} - R_M I_M, & \text{if } R \le R_M \\ V_s - R_M(\hat{I} + I_M), & \text{if } R \ge R_M \end{cases} \tag{14}$$

From this, it is trivial that the second situation would produce a more severe voltage drop at the node n, and which would be the maximum deviation from the substation voltage, V_s, since the current drawn by the other node is its maximal allowable current. In mathematical terms:

$$V_{M,min}\Big|_{N=2} = (V_s - R_M\hat{I}) - R_M I_M \tag{15}$$

Which is analogous to Eq.1 and leads then to

$$V_{M,min}\Big|_{N=2} = \frac{(V_s - R_M\hat{I}) + \sqrt{(V_s - R_M\hat{I})^2 - 4R_M P_M}}{2} \tag{16}$$

B. Application of Results: The N2-Front

An important consequence of Eq.16 is that it quantifies the lowest measured node voltage that can be observed when a power-demanding node is present on the section with another power-demanding node that is at its maximal operational point. It follows logically then that any observed voltage beyond this threshold signals the presence of *at least* three nodes on the section. This value defines the N2-front or threshold, V_{N2F}, as

$$V_{N2F} \triangleq V_{M,min}\Big|_{N=2} \tag{17}$$

In other terms:

$$\begin{cases} N > 2, & \text{if } V_M < V_{N2F} - \epsilon_p \\ \text{No information}, & \text{if otherwise} \end{cases} \tag{18}$$

Since, under extreme conditions, the N2-front can already be more than 100V away from V_σ, it is not practical to extend this methodology to estimate the presence of more than 3 nodes, as that could unhelpfully contain most of the operating voltage range. The following section presents a new methodology for that purpose.

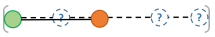

Fig. 7. The case of a node of interest is at a known distance from the substation, and no other information is known about the possible other node(s).

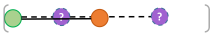

Fig. 8. The case of a node of interest at a known distance from the substation together with two other nodes on the section at an unknown position and at maximum operating conditions.

V. The $N > 3$ Region

Now, assuming there are N load nodes on the section, like in Figure 7. The nodal voltages and currents can be expressed by:

$$\mathbf{V} = -\mathbf{RI} + \mathbf{V}_s \tag{19}$$

where $\mathbf{V}$ and $\mathbf{I}$ are the Nx1 vectors of voltages and currents, respectively, and $\mathbf{R}$ is the NxN branch resistance matrix, similar to the concept of an admittance matrix, and built by applying Kirchhoff's voltage law. $\mathbf{V}_s$ is an Nx1 vector holding the substation voltage value. An example of a 3×3 (i.e., N=3) system is:

$$\begin{bmatrix} V_1 \\ V_2 \\ V_3 \end{bmatrix} = -\begin{bmatrix} R_1 & R_1 & R_1 \\ R_1 & R_1+R_2 & R_1+R_2 \\ R_1 & R_1+R_2 & R_1+R_2+R_3 \end{bmatrix} \begin{bmatrix} I_1 \\ I_2 \\ I_3 \end{bmatrix} + \begin{bmatrix} V_s \\ V_s \\ V_s \end{bmatrix} \tag{20}$$

The branch resistance can be understood as the line resistance per SI unit length, ρ, multiplied by the branch length $\mathbf{X}$.

$$\mathbf{V} = -\rho\mathbf{XI} + \mathbf{V}_s \tag{21}$$

For the sake of an example in this paper, assume a constant velocity profile, with a vector velocity $\mathbf{v}$ and initial position $\mathbf{X_0}$, the branch length vector can be rewritten so that:

$$\mathbf{V} = -\rho(\mathbf{v}t + \mathbf{X_0})\mathbf{I} + \mathbf{V}_s \tag{22}$$

Taking the derivative with respect to time,

$$\frac{\partial \mathbf{V}}{\partial t} = \frac{\partial}{\partial t}(-\rho\mathbf{v}\mathbf{I}t - \rho\mathbf{X_0}\mathbf{I} + \mathbf{V}_s) \tag{23}$$

Which can be developed into:

$$\frac{\partial \mathbf{V}}{\partial t} = -\rho\mathbf{v}\mathbf{I} - \rho\mathbf{v}t\frac{\partial}{\partial t}\mathbf{I} - \rho\mathbf{X_0}\frac{\partial}{\partial t}\mathbf{I} + 0 \tag{24}$$

A. The Case of $\forall k \neq n$ at Extreme Operational Conditions

Let the interest be now focused on a specific node, n, to study the maximum effect on its voltage variation brought by the extreme velocity and power operational conditions of all nodes k other than n (i.e., $\forall k \neq n$). This is represented in Figure 8. For the short studied duration, assume that the power demand, velocity, and node order of node n do not change significantly during the evaluation period. This complete set of conditions and assumptions can be summarized as follows:

$$\begin{cases} \frac{\partial}{\partial t}P_n \approx 0 & \text{, for the studied duration} \\ \frac{\partial}{\partial t}v_n \approx 0 & \text{, for the studied duration} \\ V_k(t=0) \triangleq V_{k,0}, & \text{Initial voltage } \forall k \\ i_k = \hat{I}, & \forall k \neq n \\ v_k = \hat{v}, & \forall k \neq n \end{cases} \tag{25}$$

For the sake of example, below follows a detailed derivation of Eq. 24 for the case of $n = 1$.

$$\frac{\partial}{\partial t}V_1 = -\rho(v_1 i_1 + 2v_1\hat{I}) - \rho[v_1 v_1 v_1]\begin{bmatrix}\frac{\partial}{\partial t}i_1\\0\\0\end{bmatrix}t - \rho[X_{1,0}X_{1,0}X_{1,0}]\begin{bmatrix}\frac{\partial}{\partial t}i_1\\0\\0\end{bmatrix} \tag{26}$$

Leading to:

$$\frac{\partial}{\partial t}V_1 = -\rho v_1\frac{P_1}{V_1} - 2\rho v_1\hat{I} + \rho v_1 t\frac{\partial}{\partial t}(\frac{P_1}{V_1}) + \rho X_{1,0}\frac{\partial}{\partial t}(\frac{P_1}{V_1}) \tag{27}$$

Finally:

$$\frac{\partial}{\partial t}V_1 = \underbrace{-\rho v_1 P_1}_{\alpha}\frac{1}{V_1}\underbrace{-2\rho v_1\hat{I}}_{\beta} - (\underbrace{-\rho v_1 P_1}_{\alpha}\,t\,\underbrace{-\rho X_{1,0}P_1}_{\gamma})\frac{1}{V_1^2}\frac{\partial V_1}{\partial t} \tag{28}$$

This same derivation can be repeated for any other position of the node n between 1 and N, giving a differential equation of the form:

$$\frac{\partial}{\partial t}V_n = \alpha\frac{1}{V_n} + \beta - (\alpha t + \gamma)\frac{1}{V_n^2}\frac{\partial V_n}{\partial t} \tag{29}$$

For which the general solution for any n is

$$V_n(t) = (-\frac{\gamma_n}{2V_{n,0}} + \frac{V_{n,0}}{2}) + \frac{\beta_n t}{2} + \frac{\sqrt{4(\alpha_n t + \gamma_n) + (\frac{\gamma_n - V_{n,0}(\beta_n t + V_{n,0})}{V_{n,0}})^2}}{2} \tag{30}$$

where the terms α_n, β_n, and γ_n are given by:

$$\alpha_n = -\rho\left(\sum_{k=1}^{n} v_k\right)\cdot P_n \tag{31}$$

$$\beta_n = -\rho\hat{I}\left(\sum_{k=1}^{n}(N-k)v_k\right) \tag{32}$$

$$\gamma_n = -\rho\left(\sum_{k=1}^{n} X_{k,0}\right)\cdot P_n \tag{33}$$

Yet a more interesting insight is offered by the derivative of V_n with respect to time:

$$\frac{\partial V_n}{\partial t} = \frac{\beta_n}{2} + \frac{\partial}{\partial t}\left(\frac{\sqrt{4(\alpha_n t + \gamma_n) + (\frac{\gamma_n - V_{n,0}(\beta_n t + V_{n,0})}{V_{n,0}})^2}}{2}\right) \tag{34}$$

Which leads to:

$$\frac{\partial V_n}{\partial t} = \frac{\beta_n}{2} + \frac{4\alpha_n + 2\beta_n^2 t - 2\beta_n(\frac{\gamma_n - V_{n,0}^2}{V_{n,0}})}{4\sqrt{4(\alpha_n t + \gamma_n) + \left(\frac{\gamma_n - V_{n,0}^2}{V_{n,0}}\right)^2 + \beta_n^2 t^2 - 2\beta_n(\frac{\gamma_n - V_{n,0}^2}{V_{n,0}})t}} \tag{35}$$

Some simplifications can be made regardless of the transport system in the study as the values of line resistance per unit length are at the order of $\mathcal{O}(10^{-4})$ (in SI units), the line current at, or higher than, $\mathcal{O}(10^2)$, the vehicle velocity at the order of $\mathcal{O}(10^1)$, the section lengths at the order of $\mathcal{O}(10^3)$, and the power at the order of $\mathcal{O}(10^5)$ or even higher [1], [2]. Consequently, $\mathcal{O}(\alpha_n) = \mathcal{O}(10^2)$, $\mathcal{O}(\beta_n) = \mathcal{O}(10^0)$, and $\mathcal{O}(\gamma_n) = \mathcal{O}(10^4)$ or $\mathcal{O}(10^5)$ depending on n. The important consequence is that the derivative can be thereby simplified to:

$$\frac{\partial V_n}{\partial t} \approx \frac{\beta_n}{2} + \frac{4\alpha_n - 2\beta_n(\frac{\gamma_n - V_{n,0}^2}{V_{n,0}})}{4\sqrt{4\gamma_n + \left(\frac{\gamma_n - V_{n,0}^2}{V_{n,0}}\right)^2}} \tag{36}$$

where the denominator can be simplified to allow writing

$$\frac{\partial V_n}{\partial t} = \frac{\beta_n}{2} + \frac{4\alpha_n - 2\beta_n(\frac{\gamma_n - V_{n,0}^2}{V_{n,0}})}{4\sqrt{\left(\frac{\gamma_n + V_{n,0}^2}{V_{n,0}}\right)^2}} \tag{37}$$

Leading to

$$\frac{\partial V_n}{\partial t} = \frac{1}{2}\beta_n\left(1 - \frac{\gamma_n - V_{n,0}^2}{\gamma_n + V_{n,0}^2}\right) + \frac{\alpha_n V_{n,0}}{\gamma_n + V_{n,0}^2} \tag{38}$$

Or ultimately to:

$$\frac{\partial V_n}{\partial t} = \frac{\beta_n V_{n,0}^2 + \alpha_n V_{n,0}}{\gamma_n + V_{n,0}^2} = \text{constant!} \tag{39}$$

The benefit of this equation is that it offers a constant value benchmark for the rate of change in voltage over a short period of time at the node of interest n, allowing to re-write the partial differential as a constant slope equation:

$$\frac{\Delta V_n}{\Delta t} = \frac{\beta_n V_{n,0}^2 + \alpha_n V_{n,0}}{\gamma_n + V_{n,0}^2} \quad (\text{for } \Delta t \leq 10\ s) \tag{40}$$

B. A Comment on the Computation of γ_n

A concern that can be raised is that the parameter γ_n requires knowledge of the original positions of the other load nodes on the section. While this information is not known, it is still reassuring that the sensitivity of the multi-variable Eq.40 with respect to the variable γ_n, given by

$$\frac{\partial}{\partial \gamma_n}\frac{\Delta V_n}{\Delta t} = -\frac{\beta_n V_{n,0}^2 + \alpha_n V_{n,0}}{(\gamma_n + V_{n,0}^2)^2} \tag{41}$$

is at the order of $\mathcal{O}(10^{-5})$. Consequently, the propagation of error from the $\sum_{k=1}^{n} X_{k,0}$ term, whose elements are the order of $\mathcal{O}(10^3)$, into Eq. 40, is at the order of $\mathcal{O}(10^{-2})$ or $\mathcal{O}(10^{-1})$.

Fortunately, the error in assuming the original position of the other nodes $\forall k \neq n$ can be easily compensated for. One possible suggestion is to use an averaged approach around the known $X_{n,0}$ term, suggested as

$$\gamma_n = -\rho\left(\sum_{k=1}^{n} X_{k,0}\right)\cdot P_n \approx -\rho(\frac{n+1}{2})X_{n,0}\cdot P_n \tag{42}$$

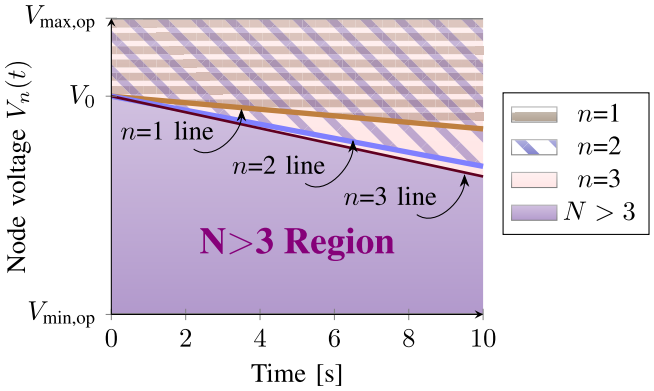

Fig. 9. Visual Representation of the $N > 3$ Region for the example in Section V-C. At any time t, a measured node voltage $V_n(t)$ that falls in the purple $N > 3$ region indicates that more than three buses are on the studied section.

It is perhaps worth mentioning again that this is not an argument against the influence of γ_n on Eq.40, but rather on the sensitivity of ΔV_n to an error in the approximation of the initial positions of all nodes k other than n. Indeed, Eq.42 is not to be understood then as an invitation to ignore the term γ_n in Eq.40, but as a validation of the offered simplification.

C. Application of Results: The $N > 3$ Region

The derivations presented in this section allow, for any studied node position, velocity, and power, to delimit the n-lines and the $N > 3$ region of this node.

To explain the meaning and utility of these lines, an example is presented in Figure 9 for a bus moving from X=1000m from the substation, away at 10m/s, and drawing 100kW.

Since the presented equations in this section of the paper consider the worst-case scenarios for the two other nodes on the studied grid section, any measured node voltage $V_n(t)$ that falls in the purple $N > 3$ region would signal the presence of more than 3 nodes on this grid section. The $N > 3$ region is described mathematically as the region between the minimum operating voltage of the grid, $V_{\text{min,op}}$, and the $V_3(t)$ node voltage described in this section when setting $n = 3$. The latter is presented in the figure as the "$n = 3$ line".

However, the other nodes could be operating at conditions more favorable than the worst-case conditions, even up to regenerative mode. Consequently, the zone between the maximum operating voltage of the grid, $V_{\text{max,op}}$, and the "$n = 3$ line" does not offer reliable information on the number of nodes on the section, and should not be used for this purpose.

In the event that reliable information is available for a particular grid zone (e.g., historically knowing that there would never be more than 3 nodes on this section), then the n-lines could offer information on the position of the studied node with respect to the two other nodes. For example, consider that the studied node is that of stationary storage, and historical information guarantees the presence of only two vehicles on this section at this time. It can follow that a measured node voltage falling between lines $n = 1$ and $n = 2$ signals to the storage system that there is at least one of the vehicles between it and the substation. This information is very useful

Fig. 10. The case when the node of interest (orange) is the first load node and at a known, close distance to the substation (green). No other information is known about the other node(s).

when estimating the load demand on the section, as explained in the coming section of this paper.

VI. Approximation of the Spare Traction Substation Power Capacity

Revisiting the equation for a single bus, an approximation can be extended for the case of two or more buses by lumping the effect of other loads on the section and their position into a grid Γ factor, namely Γ_G, and introducing it as a disturbance to the bus Γ_σ factor as follows:

$$V_M = \frac{V_s + \sqrt{V_s^2 - 4(\Gamma_\sigma + \Gamma_G)}}{2} \tag{43}$$

where V_M is the measured node voltage. Re-arranging the above equation,

$$\Gamma_G = V_M(V_s - V_M) - \Gamma_\sigma \tag{44}$$

Or finally

$$\Gamma_G = (V_\sigma - V_M)(V_\sigma + V_M - V_s) \tag{45}$$

Equation 45 can then be extended to allow an approximation of the grid support (from a storage system, for example) to be added, Γ_a, to reach the voltage level of V_σ:

$$V_M = \frac{V_s + \sqrt{V_s^2 - 4(\Gamma_\sigma + \overbrace{\Gamma_G + \Gamma_a}^{\text{aim is} \approx 0})}}{2} \tag{46}$$

Yet more generally, this approach can offer insight into the spare grid capacity or the needed grid support to reach a desired voltage V^* which is not necessarily V_σ. This is useful if, for example, a traction-grid-connected EV charger needs to estimate the available power it can draw while staying above a minimum voltage threshold.

$$V_M = \frac{V_s + \sqrt{V_s^2 - 4(\Gamma_\sigma + \Gamma_G + \Gamma_a)}}{2} \tag{47}$$

whereby Γ_a can be expressed as:

$$\Gamma_a = -(V^* - V_M)(V^* + V_M - V_s) \tag{48}$$

A powerful application of this derivation is the ability to estimate the total power demand on a traction substation. While this seems like a straightforward solution, it is important to remember that the Γ parameter is a product of power and impedance, and further work is required to attempt to decouple the power information from the Γ variable. This decoupling work is presented in the following subsections, looking at the three possible scenarios of the position of the studied node n in relation to the substation and the other power nodes.

Fig. 11. The case when one node possibly exists between the node of interest (orange) and the substation (green).

A. The Case of n=1

For the case when the node of interest is the closest to the substation, an accurate estimation of the substation demand is obtained by setting V^* to the value of V_s. In such a scenario, the voltage drop between the substation and the first node is 0 ($=V_s - V_s$), meaning that no current flows between the substation and node 1, as if the node itself is supplying all the loads on the section had its voltage been V_s.

The effectiveness of this method can be validated by recognizing the similarity between this case and the mere presence of an equivalent feeder cable before node 1. Indeed, node 1 has all the information needed about the substation current demand caused by the other nodes as it experiences a voltage drop caused by this aggregated demand.

It can be said of this system that the state of every node is not *separately observable* by node 1; however, their lumped effect is perfectly observed. This allows the reader to avoid the approximation of Eq.45 and to return to an extension of Eq. 1 for calculating the spare substation capacity as:

$$P_r = P_{spare}\Big|_{n=1} + V_s \cdot I_s\Big|_{n=1} \tag{49}$$

Or, ultimately:

$$P_{spare}\Big|_{n=1} = P_r - V_s \frac{(V_s - V_M)}{R_\sigma} \tag{50}$$

Since it follows logically from Ohm's law that if $n = 1$, then the substation current, I_s, is observed fully through the voltage drop between the substation voltage and the measured voltage of the first node over the resistance that separates them.

This is particularly interesting when, for example, the storage is placed near the traction substation or when a bus with on-board storage sees that it is *sufficiently* close to the substation. The threshold for this closeness is a design question of a statistical nature, which is a function of the total section length and the average section traffic. This is then an application-specific design decision to be made by the stakeholders.

B. The Case of n ≠ 1

The case $n \neq 1$ means at least one node exists on the section between the substation and the node of interest. Thereby, setting V^* to the value of V_s would not produce the same "blocking out" effect as previously attained.

It could be worth mentioning for the interested reader that this case becomes synonymous with the case of a bilaterally connected substation described in [5] (the case of two traction substations feeding one section), with our interest node being a *virtual* bilateral substation.

In any case, it can be argued then that if V^* is set to the value of V_s, the power share between the substations is obtained from simple circuit analysis as the ratio of the branch impedances between the load node and the two substations. Unfortunately, the position of the load node is unknown, and as a consequence, neither is this ratio of impedances.

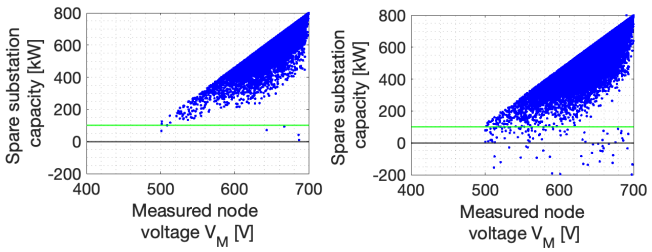

(a) Case of N=2 (b) Case of N=4

Fig. 12. Stochastic distribution of the spare trolleybus traction substation capacity as a function of the measured node voltage for 100000 grid simulations of (a) 2 load nodes and (b) 4 load nodes. The two plots have the same upper-envelope slope and are mostly populated by data above the (green) 100 kW line.

This brings the analysis back to a Γ value where, at best, an estimate can be offered for the product of the branch resistance and power of a node, but the information cannot be decoupled into the two parameters. However, some information can be inferred from a stochastic analysis. Figure 12 shows the stochastic distribution of the spare trolleybus traction substation capacity ($= P_r - V_s \cdot I_s$) as a function of the measured node voltage for 100000 stochastic grid simulations. Figure 12a shows the case of 2 load nodes, while Figure 12b studies 4 load nodes. Both figures look at simulations under the DTC of this paper. In both figures, the measured node is at the end of the line, at 1200m, to look at the worst-case scenario in terms of grid state observability (previously addressed in section IV). The measured node power demand is randomly selected between 0 and 200 kW. The first observation from Figure 12 is the existence of a linear upper envelope. The slope of this line can be shown, in fact, to be described by Eq.50. This follows logically, as the linear Eq.50 describes the least-conservative, most-observant state estimation, and all other possible grid states would, in reality, have a lower spare grid capacity.

C. Application: Power Cones

This section proposes one possible methodology for estimating the grid spare capacity using the spare-capacity cones introduced above. The derivations are conducted for a full-cone geometry but should be adapted to the specific total node number, N, expected at a section.

The cones of Figure 12 can be approximated by Figure 13, for a measured node voltage V_M that is bound by an upper limit V_U and a lower limit V_L. These limits are a case-specific design choice and particularly useful when the estimation is not done continuously, for example, by a traction-grid-connected EV charger that only estimates the grid state every 5 seconds. Such limits would thereby consider the possible zone of voltages that the estimator can see when it "wakes up" at the next estimation step. The cone crosses the zero spare capacity line at the voltage V_{ZP}, defined by setting Eq.50 equal to zero:

$$V_{ZP} \triangleq V_s - \frac{P_r R_\sigma}{V_s} \tag{51}$$

This is the most conservative voltage level at which there is no spare capacity left as it translates to the scenario where the measured node and its caused line transmission losses

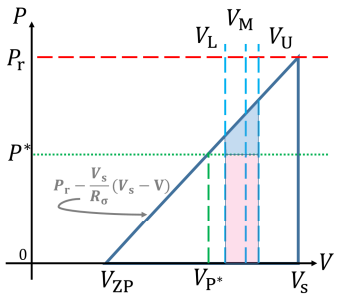

Fig. 13. The cone suggested in this paper.

consume the substation capacity completely. The simulations of Figure 12 show that this extreme scenario is never reached in practice, as most values are above the 100kW (green) line.

Consider now a desired spare capacity level, P^*. Define C_{TZ} as the number of possibilities (blue dots of Figure 12) in the trapezoid formed by the V_L line, V_U line, the upper envelope, and the P^* line (blue trapezoid in Figure 13). C_R is defined as the number of dots in the rectangle formed by the V_L line, V_U line, the P^* line, and the zero spare capacity line (pink rectangle in Figure 13). In case the voltage associated with P^*, namely V_{P^*}, is higher than V_L, then it is more accurate to speak of a C_{TR} count of the cases inside the triangle formed by the V_{P^*} line, V_U line, the upper-envelope of the cone, and the P^* line, together with C_{R,VP^*} as the number of cases in the rectangle formed with V_{P^*}.

It can be proposed then that the probability of having *at least* a P^* amount of spare traction substation capacity when seeing a node voltage of V_M is

$$p(P \geq P^*) = \begin{cases} \dfrac{C_{TZ}}{C_{TZ} + C_R}, & \text{if } V_{P^*} < V_L \\ \dfrac{C_{TR}}{C_{TR} + C_{R,VP^*}}, & \text{if } V_{P^*} \geq V_L \end{cases} \quad (52)$$

The difference between figures 12a and 12b shows how the higher traffic substations tend to populate their cones more evenly, while the lower traffic substations have a more dense distribution. If preferred, then, for the high-traffic substations, the probability can be easily (albeit less accurately) by a ratio of areas of the geometric entities previously defined. If A_{TZ} is the area of the blue trapezoid,

$$A_{TZ} = \left[P_r - \frac{V_s^2}{R_\sigma} + \frac{V_s}{2R_\sigma}(V_U + V_L) - P^* \right](V_U - V_L) \quad (53)$$

and A_{TR} is the area of the V_{P^*} triangle,

$$A_{TR} = \frac{1}{2}\left[P_r - \frac{V_s}{R_\sigma}(V_s - V_U) - P^* \right](V_U - V_{P^*}) \quad (54)$$

and A_R is the area of the pink rectangle,

$$A_R = P^* \cdot (V_U - V_L) \quad (55)$$

and A_{R,VP^*} is the area of the V_{P^*} rectangle,

$$A_{R,VP^*} = P^* \cdot (V_U - V_{P^*}) \quad (56)$$

Then it can be said that, for high-traffic substations,

$$p(P \geq P^*)\Big|_{N \gg 1} \approx \begin{cases} \dfrac{A_{TZ}}{A_{TZ} + A_R}, & \text{if } V_{P^*} < V_L \\ \dfrac{A_{TR}}{A_{TR} + A_{R,VP^*}}, & \text{if } V_{P^*} \geq V_L \end{cases} \quad (57)$$

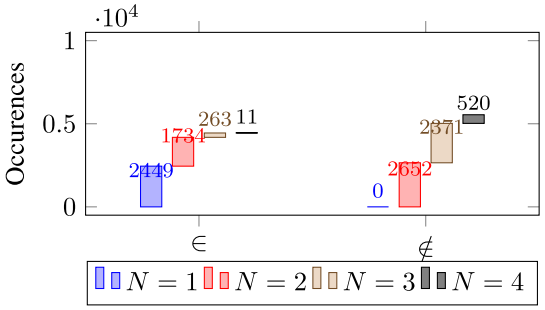

Fig. 14. Results of 10000 stochastic simulation tests of the V_σ condition introduced in Eq.13 with up to $N = 4$ nodes. As expected, triggering $V_M \notin [V_\sigma - \epsilon_p, V_\sigma[$ always correctly notifies of the presence of more than 1 node, while $V_M \in [V_\sigma - \epsilon_p, V_\sigma[$ does not offer information.

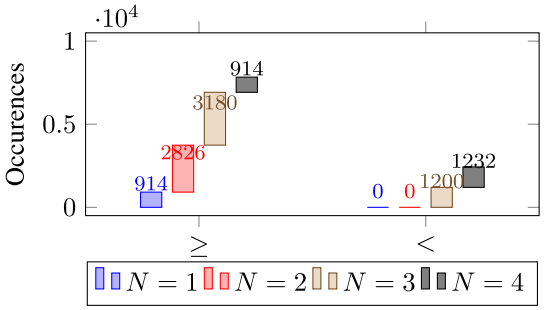

Fig. 15. Results of 10000 stochastic simulation tests of the V_σ condition introduced in Eq.18 with up to $N = 4$ nodes. As expected, triggering $V_M < V_{N2F} - \epsilon_p$ always correctly notifies of the presence of more than 2 nodes, while otherwise, no information can be deduced.

VII. Validation of the Proposed Methods Through Stochastic Simulations

A. V-Sigma Concept

Figure 14 shows the results of 10000 stochastic simulation tests of the V_σ condition introduced in Eq.13 with up to $N = 4$ nodes. The simulation parameters are according to the DTC of this paper, with ϵ_p set as 6V according to the outcome of Figure 5.

As expected, every $V_M \notin [V_\sigma - \epsilon_p, V_\sigma[$ correctly signals the presence of more than 1 node, as there are no cases when this occurs while $N = 1$. Meanwhile, $V_M \in [V_\sigma - \epsilon_p, V_\sigma[$ does not offer information on the number of nodes as there are times when it is flagged for any N between 1 and 4.

The performance of this method (desired number of flags over total cases) is then 74%, with no false flags (false positive).

B. N2-Front

Figure 15 shows the results of 10000 stochastic simulation tests of the V_{N2F} condition introduced in Eq.18 with up to $N = 4$ nodes. The simulation parameters are according to the DTC of this paper, with ϵ_p set as 6V according to the outcome of Figure 5.

As expected, triggering $V_M < V_{N2F} - \epsilon_p$ always correctly notifies of the presence of more than 2 nodes, while otherwise, no information can be deduced The performance of this method (desired number of flags over total cases) is then 37%, with no false positives. It is therefore advised to use it only in conjunction with other methods.

TABLE I

RESULTS OF 10000 STOCHASTIC SIMULATION TESTS OF THE $N > 3$ REGION INTRODUCED IN FIGURE 9 AND EQ.39. THE GREATLY SIMPLIFIED EQ. 39 DETECTS 76% OF THE CASES OF THE PRESENCE OF MORE THAN THREE NODES, AT THE COST OF 2% IN FALSE POSITIVES

	$N > 3$	$N = 3$	$N < 3$
Flagged	1649	228	0
Unflagged	535	3327	4261
Total cases	2814	3555	4261
Performance*	**76%**	**98%**	**100%**

*Desired behavior (green) over total cases

C. N3-Region

To test the "N3-region" hypothesis for the $N > 3$ case, 10000 stochastic simulations of 10 seconds were run with up to $N = 5$ nodes placed on a section under the DTC of this paper. The power ramp-up is taken as a random number between 0 and 25kW, with an upper cap per node at 300kW. The parallel line error adopted, ϵ_p, is again of 6V. The greatly simplified Eq. 39 detects 76% of the cases of the presence of more than three nodes, at the cost of 2% in false positives, as seen in Table I.

VIII. SUGGESTED EXTENSIONS OF THE GRID ESTIMATOR

A. Addressing Other Traction Section Architectures: Timetables

The derivations in this paper were presented for the most common cases of a substation feed-in at the start of the section, rather than the cases when a feed-in point can be connected somewhere along the section. Having all the nodes on the same *side* of the section offers the necessary observability to the node of interest through the voltage drops and the non-linearity in the current demand, which is key for these derivations. Another possibility is that one substation could be feeding 2 sections (or rarely, more).

One suggestion is to include the vehicle timetable -and expected delays- in the estimation of the spare power capacity. In future work, this estimator can be extended that uses the grid dynamics as input to new estimation methods.

B. Addressing Other Uncertainties: Heuristics

Another extension of the estimator can rely on heuristic approaches to the grid behavior. Heuristics are calculated guesses derived from previous experiences. Examples of such methods could be:

- Expecting a low spare power capacity in the moments after a sharp rise in line voltage: An acceleration will be coming after this regenerative braking
- Expecting that the node count has gone from N to $N-1$ after a stepwise rise in voltage: A node has left the section (and from N to $N+1$ after a stepwise drop)
- Expecting a lower certainty in the cones calculations as the line voltage rises slowly: A node is moving closer to the substation, and the effect of its presence will soon be masked from other nodes

C. Addressing Uncertainties in Incomplete Measurements

The collected local data at a power node may be incomplete due to some uncontrollable factors. It would be interesting then to expand this estimator in the future, taking into account uncertainties in the inputs.

Some works already exist on this topic in the literature, such as Latent Factor Analysis. For instance, The work in [34] proposes an alternating-direction-method of multipliers (ADMM)-based symmetric non-negative latent factor analysis (ASNL) model for correctly representing the symmetry and efficiently handling the incomplete data of large-scale undirected weighted networks. Additionally, the work in [35] proposes an efficient latent factor analysis model by a momentum-incorporated parallel stochastic gradient descent-based learning scheme, while [36] proposes a prediction-sampling-based multilayer-structured latent factor (PMLF) model for performing highly accurate representation learning on a high-dimensional and incomplete (HDI) matrix.

IX. EXAMPLES OF APPLICATIONS OF THE SUGGESTED ESTIMATOR

- Stationary Storage Systems: Can benefit from the estimator spare capacity calculations to know when to charge/discharge
- Stationary Storage Systems with distributed renewables: As above, but can also better plan the charge/discharge to increase the direct utilization of AC-side connected renewable energy systems. When renewables are on the DC side, the estimator can already pick-up on the excess energy via the voltage rises.
- Overhead-line-connected EV chargers: Can benefit from the estimator spare capacity calculations to know when to charge -or discharge if with V2G
- In-Motion-Charging buses: IMC buses are a new generation of buses that are a hybrid between trolleys (catenary supply) and battery electric buses (battery supply). They typically move under the catenary while charging with a fixed value of up to 240 kW, depending on the city, but most cities only charge conservatively as low as 100 kW. IMC buses can benefit from the estimator spare capacity calculations to know how much is available for it to charge at *any given moment* rather than a fixed value per year per city. It can also use the node number estimation to hold back if it detects the presence of another IMC bus on the section. This can significantly support the electrification of bus lines without the need for additional grid infrastructure by better utilizing the spare grid capacity.

X. CONCLUSION

This paper presented an extensive set of equations and conditions to help estimate the number of load nodes and spare grid capacity in traction substations. The methods do not require any additional sensors to be installed, which would be otherwise expensive and required to communicate reliably with each other. Up to 76% of the monitored cases were detected when validating the results with 10000 to 100000 stochastic test simulations of a verified and validated

trolleygrid model, with all but one case accurately showing zero false positives (2% in the other case). Finally, some application examples were offered for the implementation of this estimator for the integration of smart grid components into traction grids, making them more sustainable, efficient, and able to electrify more fleets without the need for additional infrastructure.

REFERENCES

[1] I. Diab, A. Saffirio, G. R. C. Mouli, A. S. Tomar, and P. Bauer, "A complete DC trolleybus grid model with bilateral connections, feeder cables, and bus auxiliaries," *IEEE Trans. Intell. Transp. Syst.*, vol. 23, no. 10, pp. 19030–19041, Oct. 2022.

[2] M. Bartłomiejczyk, *Dynamic Charging of Electric Buses*. Gdańsk, Poland: Gdańsk Univ. Technoligy, Faculty of Electrical and Control Engineering, 2018. [Online]. Available: https://books.google.cz/books?id=ziX_vQEACAAJ

[3] trolley:Motion. (2020). *trolley: Motion*. [Online]. Available: https://www.trolleymotion.eu/

[4] I. Diab, B. Scheurwater, A. Saffirio, G. R. Chandra-Mouli, and P. Bauer, "Placement and sizing of solar PV and wind systems in trolleybus grids," *J. Cleaner Prod.*, vol. 352, Jun. 2022, Art. no. 131533.

[5] I. Diab, G. R. C. Mouli, and P. Bauer, "Increasing the integration potential of EV chargers in DC trolleygrids: A bilateral substation-voltage tuning approach," in *Proc. Int. Symp. Power Electron., Electr. Drives, Autom. Motion (SPEEDAM)*, Jun. 2022, pp. 264–269.

[6] Š. Hamacek, M. Bartłomiejczyk, R. Hrbáč, S. Mišák, and V. Stỳskala, "Energy recovery effectiveness in trolleybus transport," *Electr. Power Syst. Res.*, vol. 112, pp. 1–11, Jul. 2014.

[7] D. He et al., "An integrated optimization model of metro energy consumption based on regenerative energy and passenger transfer," *Appl. Energy*, vol. 264, Apr. 2020, Art. no. 114770.

[8] I. Diab, A. Saffirio, G. R. Chandra-Mouli, and P. Bauer, "A simple method for sizing and estimating the performance of PV systems in trolleybus grids," *J. Cleaner Prod.*, vol. 384, Jan. 2023, Art. no. 135623.

[9] I. Diab, G. R. C. Mouli, and P. Bauer, "A review of the key technical and non-technical challenges for sustainable transportation electrification: A case for urban catenary buses," in *Proc. IEEE 20th Int. Power Electron. Motion Control Conf. (PEMC)*, Sep. 2022, pp. 439–448.

[10] A. S. Tomar, B. Veenhuizen, L. Buning, and B. Pyman, "Estimation of the size of the battery for hybrid electric trolley busses using backward quasi-static modelling," *Proceedings*, vol. 2, no. 23, p. 1499, 2018.

[11] R. Barbone, R. Mandrioli, M. Ricco, R. F. Paternost, V. Cirimele, and G. Grandi, "Novel multi-vehicle motion-based model of trolleybus grids towards smarter urban mobility," *Electronics*, vol. 11, no. 6, p. 915, Mar. 2022.

[12] Vanhool. (Oct. 2012). *A Bus for the Future, Leipzig*. Accessed: Feb. 23, 2018. [Online]. Available: http://www.trolley-project.eu/fileadmin/user_upload/download/Summit/TROLLEY_2nd_Summit_Jenne_ABusForTheFuture.pdf

[13] D. Iannuzzi, D. Lauria, and P. Tricoli, "Optimal design of stationary supercapacitors storage devices for light electrical transportation systems," *Optim. Eng.*, vol. 13, pp. 689–704, Jul. 2011.

[14] K. van der Horst, I. Diab, G. R. C. Mouli, and P. Bauer, "Methods for increasing the potential of integration of EV chargers into the DC catenary of electric transport grids: A trolleygrid case study," *eTransportation*, vol. 18, Oct. 2023, Art. no. 100271.

[15] I. Diab, G. R. C. Mouli, and P. Bauer, "Toward a better estimation of the charging corridor length of in-motion-charging trolleybuses," in *Proc. IEEE Transp. Electrific. Conf. Expo. (ITEC)*, Jun. 2022, pp. 557–562.

[16] A. Fernández-Rodríguez, A. Fernández-Cardador, A. P. Cucala, and M. C. Falvo, "Energy efficiency and integration of urban electrical transport systems: EVS and metro-trains of two real European lines," *Energies*, vol. 12, no. 3, p. 366, 2019.

[17] S. Rastegarzadeh, M. Mahzoon, and H. Mohammadi, "A novel modular designing for multi-ring flywheel rotor to optimize energy consumption in light metro trains," *Energy*, vol. 206, Sep. 2020, Art. no. 118092.

[18] R. Teymourfar, B. Asaei, H. Iman-Eini, and R. N. Fard, "Stationary super-capacitor energy storage system to save regenerative braking energy in a metro line," *Energy Convers. Manage.*, vol. 56, pp. 206–214, Apr. 2012.

[19] T. Zhang, R. Zhao, E. E. F. Ballantyne, and D. A. Stone, "Increasing urban tram system efficiency, with battery storage and electric vehicle charging," *Transp. Res. D, Transp. Environ.*, vol. 80, Mar. 2020, Art. no. 102254.

[20] T. Zhang, E. E. F. Ballantyne, R. Zhao, and D. A. Stone, "Technical and economic feasibility of increasing tram system efficiency with EV batteries," *Transp. Res. D, Transp. Environ.*, vol. 91, Feb. 2021, Art. no. 102681.

[21] P. Santos, P. Fonte, and R. Luis, "Improvement of DC microgrid voltage regulation based on bidirectional intelligent charging systems," in *Proc. 15th Int. Conf. Eur. Energy Market (EEM)*, Jun. 2018, pp. 1–6.

[22] K. Smith, L. Hunter, S. Galloway, C. Booth, C. Kerr, and M. Kellett, "Integrated charging of EVs using existing LVDC light rail infrastructure: A case study," in *Proc. IEEE 3rd Int. Conf. DC Microgrids (ICDCM)*, May 2019, pp. 1–7.

[23] T. Dragicevic, J. M. Guerrero, and J. C. Vasquez, "A distributed control strategy for coordination of an autonomous LVDC microgrid based on power-line signaling," *IEEE Trans. Ind. Electron.*, vol. 61, no. 7, pp. 3313–3326, Jul. 2014.

[24] I. Diab, G. R. C. Mouli, and P. Bauer, "Increasing the braking energy recuperation in electric transportation grids without storage," in *Proc. IEEE Transp. Electrific. Conf. Expo. (ITEC)*, Jun. 2023, pp. 1–5.

[25] R. F. Paternost, R. Mandrioli, R. Barbone, M. Ricco, V. Cirimele, and G. Grandi, "Catenary-powered electric traction network modeling: A data-driven analysis for trolleybus system simulation," *World Electr. Vehicle J.*, vol. 13, no. 9, p. 169, Sep. 2022.

[26] I. Diab, G. R. C. Mouli, and P. Bauer, "Opportunity charging of electric buses directly from a DC metro catenary and without storage," in *Proc. IEEE Int. Conf. Electr. Syst. Aircr., Railway, Ship Propuls. Road Vehicles Int. Transp. Electrific. Conf. (ESARS-ITEC)*, Mar. 2023, pp. 1–6.

[27] R. F. P. Paternost et al., "Energy storage management in support of trolleybus traction power systems," in *Proc. Int. Symp. Power Electron., Electr. Drives, Autom. Motion (SPEEDAM)*, Jun. 2022, pp. 252–257.

[28] R. E. Thomson and W. J. Emery, "The spatial analyses of data fields," in *Data Analysis Methods in Physical Oceanography*, 3rd ed. R. E. Thomson and W. J. Emery, Eds. Boston, MA, USA: Elsevier, 2014, pp. 313–424. [Online]. Available: https://www.sciencedirect.com/science/article/pii/B9780123877826000041

[29] R. Aggarwal and Y. Song, "Artificial neural networks in power systems. Part 1: General introduction to neural computing," *Power Eng. J.*, vol. 11, no. 3, pp. 129–134, Jun. 1997.

[30] X. Luo, M. Zhou, Z. Wang, Y. Xia, and Q. Zhu, "An effective scheme for QoS estimation via alternating direction method-based matrix factorization," *IEEE Trans. Services Comput.*, vol. 12, no. 4, pp. 503–518, Jul. 2019.

[31] D. Wu, P. Zhang, Y. He, and X. Luo, "A double-space and double-norm ensembled latent factor model for highly accurate web service QoS prediction," *IEEE Trans. Services Comput.*, vol. 16, no. 2, pp. 802–814, Mar. 2023.

[32] X. Luo, H. Wu, H. Yuan, and M. Zhou, "Temporal pattern-aware QoS prediction via biased non-negative latent factorization of tensors," *IEEE Trans. Cybern.*, vol. 50, no. 5, pp. 1798–1809, May 2020.

[33] R. T. Birge, "The propagation of errors," *Amer. J. Phys.*, vol. 7, no. 6, pp. 351–357, 1939.

[34] X. Luo, Y. Zhong, Z. Wang, and M. Li, "An alternating-direction-method of multipliers-incorporated approach to symmetric non-negative latent factor analysis," *IEEE Trans. Neural Netw. Learn. Syst.*, vol. 34, no. 8, pp. 4826–4840, Aug. 2023.

[35] X. Luo, W. Qin, A. Dong, K. Sedraoui, and M. Zhou, "Efficient and high-quality recommendations via momentum-incorporated parallel stochastic gradient descent-based learning," *IEEE/CAA J. Autom. Sinica*, vol. 8, no. 2, pp. 402–411, Feb. 2021.

[36] D. Wu, X. Luo, Y. He, and M. Zhou, "A prediction-sampling-based multilayer-structured latent factor model for accurate representation to high-dimensional and sparse data," *IEEE Trans. Neural Netw. Learn. Syst.*, early access, Sep. 9, 2022, doi: 10.1109/TNNLS.2022.3200009.

Ibrahim Diab (Member, IEEE) received the bachelor's degree in mechanical engineering from the American University of Beirut in 2012. He is a Ph.D. candidate at the DC systems, Energy conversion and Storage (DCE&S) group at the Department of Electrical Sustainable Energy (ESE), Delft University of Technology, The Netherlands. He then worked as a Measurement-While-Drilling engineer with Schlumberger in Saudi Arabia until August 2014. In 2015, he received the TU Delft "Delft Research Initiative - Energy" full scholarship and joined the ESE department as a master student under the Sustainable Energy Technologies (SET) masters program (2017, honors).

After graduating, he started with the DCE&S group as a full-time Teaching Assistant on courses on AC and DC Microgrids, Electrical Power Conversion, and on the System Integration project. He then worked as a Co-Creator and Manager for the Professional Certificates online courses of the ESE Department on Intelligent Electrical Power Grids, and on Electrical Power Conversion. Since July 2019, he has been working with the DCE&S group as a Ph.D. candidate on transforming the trolleybus grid into an active, sustainable, and multi-functional transport grid of the future. Since September 2022, he has been also a Research Fellow at the AMS institute in Amsterdam working on the integration of EV chargers in the metro grid of Amsterdam.

Gautham Ram Chandra Mouli (Member, IEEE) received the bachelor's degree from the National Institute of Technology, Trichy, India, in 2011, the master's degrees in electrical engineering from Delft University of Technology, The Netherlands, in 2013, and the Ph.D. degree for the development of a solar powered V2G electric vehicle charger compatible with CHAdeMO, CCS/COMBO, and designed smart charging algorithms (with PRE, ABB, and UT Austin) from the Delft University in 2018. From 2017 to 2019, he was a postdoctoral researcher at TU Delft pursuing his research on power converters for EV charging, smart charging of EVs, and trolley busses. He is the coordinator and a Lecturer for Massive Open Online Course (MOOC) on Electric cars on edX.org with 200,000 learners from 175 countries. He is a tenured Assistant Professor in the DC systems, energy conversion and storage group with the Department of Electrical Sustainable Energy, Delft University of Technology. His current research focus on electric vehicles and charging, PV systems, power electronics, and intelligent control.

Dr. Mouli was awarded the best paper prize in the IEEE TRANSACTIONS ON INDUSTRIAL INFORMATICS in 2018, the Best Poster prize at Erasmus Energy Forum 2016, The Netherlands and the Best Paper prize at the IEEE INDICON Conference 2009, India. It was awarded the 'Most significant innovation in electric vehicles' award from IDtechEx in 2018, and the 'Best Tech Idea of 2018' by KIJK. He is involved in many projects with industrial and academic partners at national and EU level concerning electric mobility and energy storage such as OSCD, Trolley 2.0, Flexinet, TULIPS, FLOW, Drive2X and NEON. He is the Vice-chair of IEEE Industrial Electronic Society Benelux chapter.

Pavol Bauer (Senior Member, IEEE) received the master's degree in electrical engineering from the Technical University of Kosice, Koisce, Slovakia, in 1985, and the Ph.D. degree from the Delft University of Technology, Delft, The Netherlands, in 1995.

He is currently a Full Professor with the Department of Electrical Sustainable Energy, Delft University of Technology, the Head of DC Systems, Energy Conversion and Storage Group, a Professor with the Brno University of Technology, Brno, Czechia, and the Honorary Professor with Politehnica University Timisoara, Timisoara, Romania. From 2002 to 2003, he was with KEMA (DNV GL, Arnhem) on different projects related to power electronics applications in power systems. He has authored and coauthored more than 120 journals and 500 conference papers in his field with H factor Google scholar 40, Web of Science 26, he is the author or coauthor of eight books, holds seven international patents and organized several tutorials at the international conferences. He has worked on many projects for industry concerning wind and wave energy, power electronic applications for power systems such as Smarttrafo, HVDC systems, projects for smart cities such as PV charging of electric vehicles, PV and storage integration, contactless charging, and participated in several Leonardo da Vinci, H2020 and Electric Mobility Europe EU projects as a Project Partner (ELINA, INETELE, E-Pragmatic, Micact, Trolley 2.0, OSCD, P2P, Progressus) and a Coordinator (PEMCWebLab.com-Edipe, SustEner, Eranet DCMICRO). His main research focuses on power electronics for charging of electric vehicles and dc grids. He is the Former Chair of Benelux IEEE Joint Industry Applications Society, Power Electronics and Power Engineering Society chapter, the Chair of the Power Electronics and Motion Control council, Member of the Executive Committee of European Power Electronics Association and the International Steering Committee at numerous conferences.